EPR investigation of TiCl3dissolved in polar solvents – implications for the understanding of active Ti(iii) species in heterogeneous Ziegler–Natta catalysts

(Article begins on next page)

10 July 2024

UNIVERSITÀ DEGLI STUDI DI TORINO

ARTICLE TYPE

EPR Investigation of TiCl$_3$ Dissolved in Polar Solvents - Implications for the Understanding of Active Ti(III) Species in Heterogeneous Ziegler-Natta Catalysts

Sara Maurelli,[a,c] Elena Morra,[a,b,c] Sabine Van Doorslaer,*[a,c] Vincenzo Busico,[c,d] Mario Chiesa*[b,c]

5

Multi-frequency continuous-wave and pulsed EPR techniques are employed to investigate Ti(III)-chloro complexes obtained by dissolving TiCl$_3$ in anhydrous and hydrated methanol. Two distinctly different species, characterized by different **g** matrices are observed in the two cases. Hyperfine sublevel correlation (HYSCORE) spectroscopy is found to be a powerful method to identify the type of nuclei
10 surrounding the Ti^{3+} ion. For the first time, the hyperfine and nuclear quadrupole data of Ti(III)-bound $^{35/37}$Cl nuclei are reported together with ^{1}H and ^{13}C hyperfine data of the coordinated methanol molecules. DFT modelling allows interpreting the measured spin Hamiltonian parameters in terms of microscopic models of the solvated species. The theoretical observable properties (**g** matrix, $^{35/37}$Cl, ^{1}H and ^{13}C hyperfine tensors) are in quantitative agreement with the experiments for two families of complexes:
15 [TiCl$_n$(CH$_3$OH)$_{6-n}$]$^{(3-n)+}$ (with n ranging from 0 to 2) and [Ti(CH$_3$OH)$_5$(OH)]$^{2+}$ or [Ti(CH$_3$OH)$_5$(OCH$_3$)]$^{2+}$. The first complex is observed in anhydrous methanol, while the second type of complexes is observed when water is added to the solution; the presence of OH$^-$ and/or CH$_3$O$^-$ species being promoted by water hydrolysis. The results obtained for the frozen solutions are critically compared to EPR spectra recorded for a MgCl$_2$-supported Ti-based Ziegler-Natta model catalyst.

20 ## Introduction

The chemistry of Ti^{3+} is very diverse and involves important chemical and photochemical reactions in both solid and liquid phases. Crystalline TiCl$_3$ for example is the prototypical solid component of the catalytic system for the selective polymerization of α-olefins.1 Ziegler-Natta catalysts have evolved from the self-supported TiCl$_3$-based catalyst originally proposed by Ziegler and Natta2 into the current MgCl$_2$-supported TiCl$_4$ systems, where catalytically active species are generated by reductive activation with different
25 alkylaluminium compounds, which play the role of co-catalysts. The catalytically active species formed on MgCl$_2$-supported TiCl$_4$ catalysts are then usually associated with isolated (diluted) Ti(III) species, whose detailed structural and electronic features are still poorly understood.

From a broad perspective, the formation of isolated Ti(III) species on the MgCl$_2$ support may be regarded as a sort of dissolution process, where the MgCl$_2$ support takes the role of a polar solid solvent - as is indeed the case in many important catalytic processes -
30 with the Ti(III) ion as the solute. This description bears comparison, both conceptually and phenomenologically, with the dissolution of solid TiCl$_3$ in liquid polar solvents. Of course, in the case of the solid-state system, the local topological details of the matrix (solvent) will have an important influence on the electronic properties and reactivity of the Ti(III) species (solute). Nevertheless, this analogy can provide some useful guidelines in the understanding of the general properties of diluted Ti(III)-chloro complexes. Bearing this in mind, it is the purpose of this work to study the EPR properties of TiCl$_3$ when the solid is dissolved in polar solvents such as methanol.

35 Due to the paramagnetic nature of Ti(III), electron paramagnetic resonance (EPR) has been widely employed in its characterization and has led to singular progresses in the understanding of its electronic and geometrical features in different environments.3 We recently employed EPR, electron nuclear double resonance (ENDOR) and electron spin-echo-envelope-modulation (ESEEM) techniques to characterize the solvation structure of Ti^{3+} ions in glassy water.4 The EPR properties of Ti(III)-chloro complexes have been relatively poorly explored in the past and in particular, except for a recent Q-band pulsed EPR study on Cp$_2$TiCl,5 the application of modern EPR
40 techniques (high-field and pulsed EPR) to these systems is lacking.

CW-EPR spectra of chloro complexes of Ti(III) have been reported by Giggenbach and Brubaker,6 while the dissolution of TiCl$_3$ in different organic bases was studied by Raynor and Ball.7 Carr and Smith8 reported EPR spectra of titanium trichloride in pyridine solutions, providing evidence for a dimeric form characterized by triplet-state spectra.

A plurality of species with general formula [TiCl$_n$(CH$_3$OH)$_{6-n}$]$^{3-}$ was assumed in the case of methanol solutions depending on the nature
45 and concentration of the solvent.6 An interesting study, aimed at clarifying the nature of Ti(III) species in alcohols-water solutions has been reported by Kuchmii et al.9 who studied the EPR and UV-Vis spectra of Ti(III) in different water/methanol mixtures at different

pH, providing evidence for the delicate role of water (even in traces) in favoring the presence of a series of labile coordination compounds with different coordination spheres and characterized by distinct CW-EPR spectra.

For some complexes the hyperfine interaction with the magnetically active ^{47}Ti and ^{49}Ti isotopes was also reported,[10] but no details are currently present about the spin density-distribution over the directly coordinate chlorine ligands. Such information can be obtained by means of so-called hyperfine techniques (ENDOR, ESEEM, HYSCORE (hyperfine sublevel correlation spectroscopy)), which allow to resolve hyperfine interactions down to sub-MHz resolution. Only few reports are available about the hyperfine interaction of paramagnetic transition-metal ions to directly coordinated chlorine ligands[11,12] and to the best of our knowledge no data are available about ^{35,37}Cl hyperfine interactions in Ti(III)-Cl-containing systems.

The aim of this work is thus to explore the EPR properties of TiCl$_3$ dissolved in methanol and methanol-water solutions. For this, CW EPR at 9.5 and 95 GHz, HYSCORE spectroscopy and DFT calculations will be combined. We specifically aim at resolving the hyperfine interactions of directly coordinated ligands containing magnetically active nuclei (in particular ^{35,37}Cl) and at correlating the occurrence of different EPR-active species with different local environments in an effort to clarify the nature of the different Ti^{3+} coordination complexes found in these solutions. Comparison with the Ti(III) EPR spectra recorded for α- and β- crystalline TiCl$_3$ and a model high yield Ziegler-Natta catalyst strongly suggests that the results obtained from the molecular Ti(III) complexes will set the basis for a better understanding of the more complex Ti(III) species on heterogeneous Ziegler-Natta catalysts.

Experimental

Sample preparation

The TiCl$_3$ solutions have been prepared in a glove box under controlled atmosphere (oxygen content < 3ppm$_V$, water content < 2.5 ppm$_V$). The violet α polymorph of TiCl$_3$ (α-TiCl$_3$) has been dissolved in anhydrous methanol. In order to study the effect of water contamination a solution was prepared by dissolving the solid in hydrated methanol obtained by exposing the anhydrous solvent to the atmosphere for two days. A sample of α-TiCl$_3$ was kindly provided by Prof. M. Terano, JAIST. Samples of β-TiCl$_3$ and a model Ziegler-Natta catalyst obtained by activation of ball-milled MgCl$_2$/TiCl$_4$ with tryethylaluminium (TEA) have been prepared according to the literature.[13]

Spectroscopic measurements

X-band continuous-wave (CW) and pulsed EPR spectra were detected on a Bruker Elexsys E580 spectrometer operating at a microwave frequency of 9.76 GHz. W-band EPR measurements were performed on a Bruker E680 spectrometer operating at 94 GHz. The EPR spectrometers are equipped with helium gas-flow cryostats (Oxford, Inc.). All experiments were performed at 10 K.

The X-band CW-EPR measurements were performed with a microwave (mw) power of 0.015 mW, a modulation frequency of 100 kHz and a modulation amplitude of 0.5 mT. For the W-band CW-EPR measurements the following experimental parameters have been used: mw power = 0. 44 µW, modulation frequency = 100 kHz.

Electron-spin-echo (ESE)-detected EPR experiments were carried out with the pulse sequence: $\pi/2 - \tau - \pi - \tau - echo$. For the X-band experiments the mw pulse lengths $t_{\pi/2}$ = 16 ns and t_π = 32 ns and a τ value of 200 ns were used, while for the W-band measurements $t_{\pi/2}$ = 92 ns and t_π = 184 ns and a τ value of 600 ns were chosen. The shot repetition time adopted for the experiments was 1 kHz.

Two-pulse ESEEM measurements were carried out at X-band by increasing the time delay τ of the pulse sequence: $t_{\pi/2} - \tau - t_\pi - \tau - echo$, with $t_{\pi/2}$ = 16ns and t_π = 32ns. 350 τ values were used, starting from 88ns with a τ-increment of 16ns. Two-dimensional two-pulse ESEEM spectra have been obtained by sweeping the magnetic field from 340mT to 400mT (301 data points). A 1 kHz repetition rate was used. Further experimental details are specified in the figures caption.

HYSCORE experiments[14] were carried out at X-band with the pulse sequence $\pi/2 - \tau - \pi/2 - t_1 - \pi - t_2 - \pi/2 - \tau - echo$ with the microwave pulse lengths $t_{\pi/2}$ = 16 ns and t_π = 32 ns. The time intervals t_1 and t_2 were varied in steps of 16 ns starting from 96 ns to 4896 ns with a repetition rate of 1 kHz. In order to avoid blind-spot effects different τ values were chosen as specified in the figure captions. A four-step phase cycle was used to eliminate unwanted echoes. The time traces of the HYSCORE spectra were baseline corrected with a third-order polynomial, apodized with a Hamming window and zero filled. After two-dimensional Fourier transformation, the absolute value spectra were calculated.

All EPR and HYSCORE spectra were simulated using the Easyspin simulation package.[15]

Computational details

The g values and hyperfine (*hfi*) and nuclear quadrupole (*nqi*) parameters were calculated for different Ti(III) model complexes using spin-unrestricted density functional computations with the ORCA computational package.[16] Geometry optimizations were performed using the BP86 functional[17] with the SVP basis set for all atoms except Ti for which a more polarized triple-ζ valence basis set (TZVPP) is used.[18] For the computation of the EPR data, different functional/basis-set combinations were evaluated for TiF$_3$ for which EPR data of the complex in neon and argon matrices are available.[19] Although none of the used combinations led to an exact reproduction of the parameters, the best results were obtained using the PBE0 functional,[20] with the triply polarized "Core Properties" (CP(PPP)) basis set for Ti [21] and TZVPP for F. Because of this, all computations on the Ti(III) complexes under study were performed using the PBE0 functional in combination with the CP(PPP) basis set for Ti, the TZVPP basis set for Cl and EPR-II[22] for all other atoms. The solvent surrounding was simulated using the COSMO model.[23]

Results

The X-band CW-EPR spectra of Ti(III) in different systems are shown in Figure 1. The spectra of α-TiCl$_3$ and β-TiCl$_3$ powders show relatively weak and ill-defined powder patterns characterized by resonances at $g \approx 1.96$. (Figure S1 ESI) Line shape and relative spectral intensities are different for the two different phases and in both cases broad features are superimposed to the main signal. For the α-TiCl$_3$ phase a magnetic moment corresponding to 1.31 BM has been measured at 300K with a Neel Temperature of 165K and corresponding onset of anti-ferromagnetism at lower temperatures.[24] For the β-TiCl$_3$ a much lower magnetic moment has been reported of 0.7 BM.[24] The strong exchange interactions characteristic of solid TiCl$_3$ lead to EPR-silent states. Therefore, it is probable that the EPR signals reported in Figure 1a and 1b are to be associated to defect states in the solid matrix.

A different, more complex EPR spectrum is obtained in the case of a model Ziegler-Natta catalyst obtained by activation with triethylaluminium (TEA) vapors of a MgCl$_2$/TiCl$_4$ pre-catalyst. The spectrum is reported in Figure 1a and features a complex EPR powder pattern indicating the presence of multiple EPR active species characterized by g values typical of isolated Ti(III) but experiencing different local environments. Quantitation of the EPR signal in Figure 1c, indicates that the amount of EPR active Ti(III) is of the order of 10±5 % of the Ti present in the sample. Given the reducing conditions, a large portion of EPR-silent reduced Ti is likely to be present, whose nature is at the moment undetermined. Similar spectra have been reported in the literature in the past[25,26] and will be the object of a forthcoming paper. In this context we limit ourselves to highlight the similarities of this spectrum with spectra observed when TiCl$_3$ is dissolved in polar liquid solvents (Figures 1 b-d).
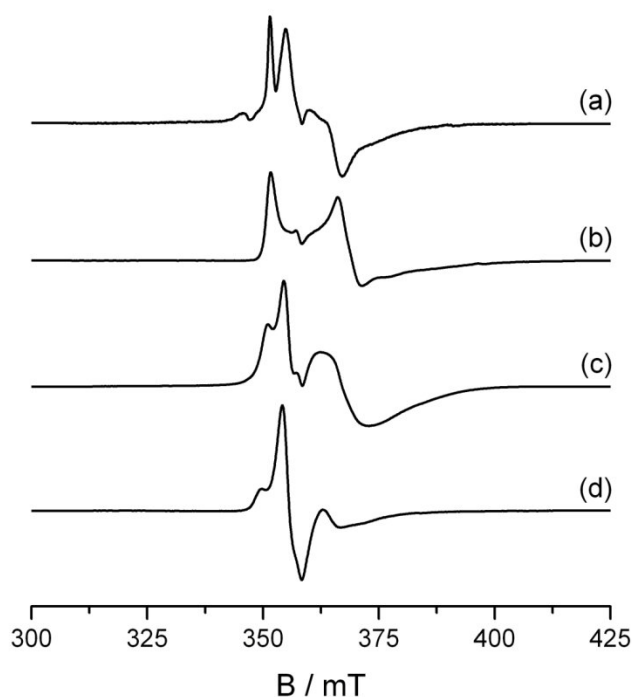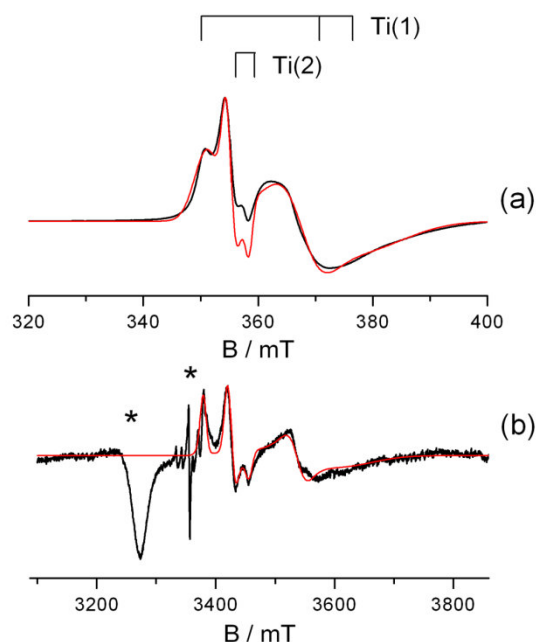

Fig. 1 Experimental X-band CW EPR spectra of (a) Ti(III) species generated in ball-milled MgCl$_2$/TiCl$_4$ upon activation with TEA, (b) frozen solution of TiCl$_3$ dissolved in dry methanol (c) frozen solution of TiCl$_3$ dissolved in hydrated methanol, (d) diluted frozen solution of TiCl$_3$ dissolved in hydrated methanol. The spectral intensities are normalized.

The dissolution of solid TiCl$_3$ in a polar solvent such as anhydrous methanol (Figure 1b) leads to an EPR spectrum which is characterized by a relatively large anisotropy, while a spectral pattern very similar to that of the model Ziegler-Natta catalyst is observed in the case of the hydrated methanol solution (compare Figure 1a and 1c). Further dilution of the TiCl$_3$-hydrated methanol solution leads to the decrease of the broad resonance absorption enhancing the contribution of a low anisotropic, narrow spectral feature. Indeed, the comparison of the CW-EPR spectra of isolated Ti(III) species in the solid and liquid phases reveal interesting similarities, which corroborate the analogy with the dissolution process in both solid and liquid systems. Dwelling on this analogy, we provide in the following a detailed EPR characterization of the frozen solutions of TiCl$_3$ in anhydrous and hydrated methanol solutions.

The EPR spectrum of TiCl$_3$ dissolved in anhydrous and hydrated methanol

The EPR spectrum of TiCl$_3$ dissolved in absolute methanol is characterized by an anisotropic powder pattern reported in Figure 1b. Simulation of the spectrum (Figure S2, ESI) indicates that the signal is dominated by a species with g_1=1.830, g_2=1.889, g_3=1.978(Species 1 in Table 1) with a minor contribution of a second species with pseudo axial symmetry and reduced anisotropy ($g_\perp$=1.962, $g_\parallel$=1.942, species 2 in Table 1). The relative abundance of the two species reported in Table 1 has been obtained by computer simulation. The spectrum is characterized by a relatively large line width broadening, in particular of the high-field spectral component,

that can be explained considering strain effects induced by a plurality of solvation structures, which slightly differ one from another and/or by $^{47/49}$Ti hyperfine interactions. A similar effect was observed in the case of hydrated Ti(III) species.[4] The measured *g* values agree well with previous literature reports (Table 1) where similar spectra have been tentatively assigned to mixed chloride-alcoholate complexes.[6,7,9]

Fig. 2 Experimental (black) and simulated (red) CW EPR spectra of TiCl$_3$ dissolved in a methanol-water mixture recorded at (a) X-band and (b) W-band frequencies. The spin Hamiltonian parameters used to simulate the experimental spectra are listed in Table 1. The stick diagram indicates the peaks corresponding to the two Ti(III) species considered in the computer simulation (Table 1). The asterisks indicate spurious W-band cavity signals.

As reported in ref. 9 a more complex spectrum is obtained by dissolving TiCl$_3$ in a methanol solution containing traces of water (Figure 1c). Computer simulation of this spectrum, recorded at two different microwave frequencies, (Figure 2) reveals that the spectrum can be rationalized in terms of the superposition of species 1 and 2 previously identified, whereby the contribution of species 2 has increased over one order of magnitude. We stress at this stage again that the X-band CW-EPR spectrum in Figure 1c shows important similarities with the spectrum observed in the case of the activated model Ziegler-Natta catalyst (Figure 1a). In the following we therefore analyze the spectrum of TiCl$_3$ dissolved in the methanol/water mixture in detail in order to clarify the nature of the contributing species (species 1 and species 2).

The onset of species 2 was reported by Kuchmii[9] to correlate with the amount of added water in ethanol-water solutions and to become the dominant species when small amounts of sodium hydroxide were added to the alcohol solution. On the basis of these observations the EPR signal associated to species 2 was assigned to hydroxo complexes of Ti(III), where OH$^-$ groups are replacing for the Cl$^-$ ligands. A large number of experimental measurements of the equilibrium constant for the H$^+$ transfer reaction:

$$H_2O + CH_3O^- \leftrightarrows HO^- + CH_3OH$$
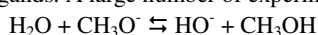
in various methanol solutions supports that methanol is at least twice as acidic as water.[27] The formation of hydroxy complexes upon water addition to the methanol solution agrees thus with the known pK_{a1} value of [Ti(H$_2$O)$_6$]$^{3+}$ which has been reported to range between 1.8 and 2 [28] making it a relatively strong acid and implying that spontaneous deprotonation of [Ti(H$_2$O)$_6$]$^{3+}$ can be expected even at acidic pH.

Table 1 Spin Hamiltonian parameters for Ti(III) complexes in different frozen solutions.

		g_1	g_2	g_3	Ab. (%)	Ref
$[Ti(H_2O)_6]^{3+}$		1.896	1.896	1.994	100	4
TiCl$_3$ / CH$_3$OH	Species 1	1.830 ± 0.080	1.889 ± 0.005	1.978 ± 0.003	99.9	This work
	Species 2	1.942 ± 0.005	1.962 ± 0.005	1.962 ± 0.005	0.1	
TiCl$_3$ / CH$_3$OH / H$_2$O	Species 1	1.830 ±0.080	1.889 ± 0.005	1.978 ± 0.003	95	This work
	Species 2	1.942 ±0.005	1.962 ± 0.005	1.962 ± 0.005	5	
TiCl$_3$ / CH$_3$OH		1.854	1.897	1.987		6
TiCl$_3$ / CH$_3$OH		1.88	1.90	1.98		7
TiCl$_3$ / C$_2$H$_5$OH		1.833	1.903	1.988		9
TiCl$_3$ / C$_2$H$_5$OH/ H$_2$O	Species 1	1.833	1.903	1.988		9
	Species 2	1.945	1.961	1.961		

In order to investigate in more detail the nature of the two Ti(III) complexes observed for TiCl$_3$ in methanol-water mixtures, pulsed EPR experiments were performed. A first hint about the magnetic nuclei surrounding the Ti(III) in species 1 and 2 was obtained from X-band field-dependent two-pulse ESEEM (Figures S3, S4 ESI). This indicated that both species have proton-rich ligands. While for species 1 additional *hfi* with ^{35,37}Cl are observed, there seems to be no chloride ligation involved in species 2. This is consistent with the evolution of the EPR spectrum as a function of TiCl$_3$ concentration in the water-methanol solution shown in Figure 1d. The intensity of the contribution of species 1, associated with the presence of coordinated chlorides, is found to decrease on lowering the TiCl$_3$ concentration, consistently with the decrease of resonating Ti-Cl species.
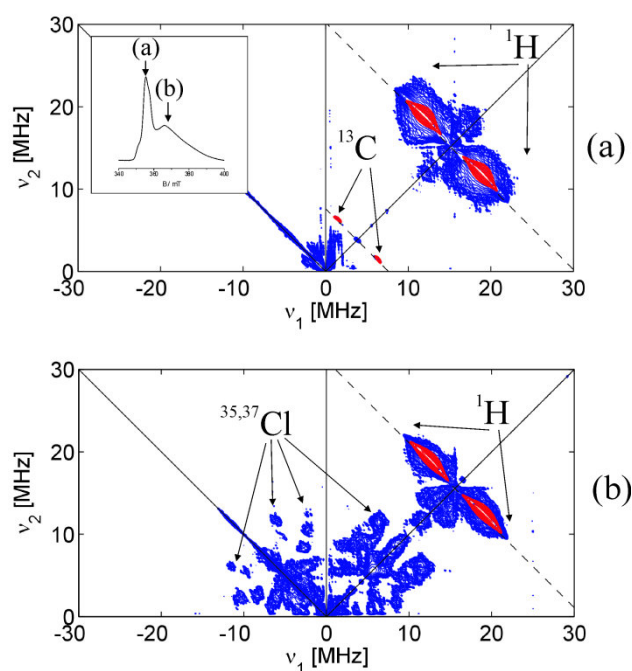
Fig. 3 Experimental (blue lines) and computer-simulated (red lines) X-band HYSCORE spectra of TiCl$_3$ dissolved in hydrated methanol. The spectra are taken at $\tau = 128$ns and field positions indicated by the arrows in the ESE-detected EPR spectrum in the inset: (a) $B_0 = 355.0$ mT, (b) $B_0 = 365.0$ mT. The parameters extracted from computer simulation of, ^{13}C and ^{1}H signals are listed in Table 2. A low contour level is set for spectrum (a) in order to visualize the ^{13}C signal (1.11% abundance). The simulation analysis of the Cl HYSCORE spectrum is reported in Figure S8 of the ESI section.

In order to further elucidate the interactions with the surrounding magnetic nuclei, HYSCORE experiments were undertaken. Distinctly different HYSCORE spectra were recorded depending on the observer positions (Figure 3), in agreement with the two-pulse ESEEM spectra (Figure S4 ESI). In particular, at a field position corresponding to the maximum of the narrow spectrum of species 2

(position (a) in the inset of Figure 3) only signals stemming from ^{1}H and ^{13}C of coordinated methanol groups are observed. The spectrum is dominated by a pronounced ^{1}H ridge with maximum extension of approximately 12 MHz. The full hyperfine tensor is obtained by means of computer simulation (Table 2 and Figure S6-S9 ESI). The values agree nicely with those reported by some of us[4] for protons of coordinated water molecules in the hexa-aquo Ti(III) complex and can be assigned to -OH protons of directly coordinated molecules (CH$_3$OH or H$_2$O) or hydroxyl ions (OH$^-$). Together with the ^{1}H ridge, the HYSCORE spectrum recorded at this field position is also characterized by the presence of two elongated cross peaks centered at the ^{13}C nuclear Larmor frequency and separated by approximately 4 MHz.

Table 2 Spin Hamiltonian parameters extracted from computer simulation of the HYSCORE spectra of TiCl$_3$ dissolved in methanol and methanol-water mixtures (Figure 3). All *hfi* and *nqi* values are in MHz, while Euler angles are given in degrees. The signs of the hyperfine and quadrupole tensors components have been chosen accordingly to the DFT computed values

|		a_{iso}	T_x	T_y	T_z	$|A_x|$	$|A_y|$	$|A_z|$	α,β,γ	Q_x	Q_y	Q_z	α',β',γ'
^{13}C	Exp.	+3.8±0.2	-0.8±0.2	-1.3±0.2	+2.2±0.4	3.0±0.2	2.5±0.2	5.9±0.2	0, 0,0	-	-	-	-
^{1}H	Exp.	+4.43±0.4	-3.9±0.2	-4.23±0.2	+8.17±0.1	0.5±0.2	0.2±0.2	12.6±0.5	0±10, 55±20, -60±5	-	-	-	-
^{35}Cl	Exp	-0.7±0.5	-5.3±0.5	-6.7±0.5	7.8±0.5	4.6±0.5	6±0.5	8.5±0.5	50±10,50±10, -30±10	+0.62 ±0.02	+0.96 ±0.03	-1.55 ±0.03	30±10,15±10 -20±10

a

The observation of two well resolved off-diagonal peaks instead of a "ridge" pattern indicates that the *hfi* has a relatively large Fermi contact contribution, suggesting a through-bond spin transfer mechanism. From computer simulation of the ^{13}C signal, an a_{iso} value of 3.8 MHz is obtained, corresponding to a 0.12% spin density in the carbon 2*s* orbital (Table 2 and Figure S7 ESI). This value is in line with the spin density transfer in the hydrogen 1*s* orbital (0.13%) estimated through the ^{1}H a_{iso} value (4.4 MHz). This observation clearly suggests the direct coordination of methanol groups where the spin-transfer mechanism over the C and H atoms of the Ti –OCH$_3$ and Ti –OH fragments is the same. The HYSCORE spectrum with predominant contributions of species 2, thus indicates that the solvation sphere of the Ti(III) ions is composed by directly coordinated methanol or methoxy groups and possibly H$_2$O or OH$^-$ groups and excludes the presence of directly coordinated Cl$^-$ ions. A sharp EPR absorption was detected by Goldberg[29] and by Waters and Maki[10] for TiCl$_3$ in methanol solutions which contained methoxy ions. Moreover, spectra of frozen solutions characterized by an asymmetric signal consisting of two lines with experimental values of $g_\perp$ = 1.960 and g_{ll} = 1.944 were tentatively assigned to a [Ti(OCH$_3$)(CH$_3$OH)]$^{2+}$ species.[6] The same EPR signal was observed also by Kuchmii and co-workers[9] who assigned the signal to tetrahedral complexes with coordinated hydroxyl groups ([TiOH(ROH)$_3$]$^+$ or [TiOH(H$_2$O)$_3$]$^+$). The assignment of the sharp EPR signal to a Ti(III) species without coordinated chlorine ions is consistent with the present HYSCORE experiments, however a firm assignment of the species will be done based on DFT calculations (*vide infra*).

The spectrum recorded at a magnetic field setting corresponding to the maximum of the broad signal associated to species 1 (position b in the inset of Figure 3) is shown in Figure 3b. Also in this case the pronounced ^{1}H ridge is present, indicating the presence of directly coordinated CH$_3$OH molecules, but a number of additional cross peaks are now clearly observed in both quadrants. This complex spectral pattern is clearly associated to the interaction of the unpaired electron with ^{35,37}Cl nuclei (*I*=3/2). The interpretation of HYSCORE spectra for high spin nuclei presents a number of difficulties. Moreover in the case of chlorine two stable isotopes, ^{35}Cl and ^{37}Cl, both characterized by *I*=3/2 but with different nuclear quadrupole moments are present, which further complicate the assignment and interpretation of the spectrum.

The interpretation of HYSCORE spectra from ligand chlorine nuclei presents thus a number of challenges which make it very difficult to obtain the spin Hamiltonian parameters based on qualitative considerations and direct simulation of the spectra, as is usually done in the case of simpler systems. To overcome these difficulties we used DFT calculated parameters for different [TiCl$_n$(CH$_3$OH)$_{6-n}$]$^{(3-n)+}$ species (*vide infra*) as starting points for the numerical simulation of the HYSCORE spectrum. We base the models on earlier suggestions by Giggenbach[6] who assigned the CW-EPR spectrum of species 1 to the complex [Ti(Cl$_2$(CH$_3$OH)$_4$]Cl based on the EPR and UV-Vis absorption spectra of different polycrystalline chloro-methanol complexes of Ti(III). In particular, given the high number of parameters, which are needed to simulate the HYSCORE spectrum of Cl, we used the Euler angles extracted from DFT computations and searched for the eigenvalues of the *hfi* and *nqi* tensors, using the computed values as starting point. We then optimized the Euler angles. The result of this simulation analysis performed for spectra recorded at different magnetic field settings is reported as supplementary information (Figure S8 ESI), while the corresponding set of spin Hamiltonian parameters is listed in Table 2. Only a single Cl nucleus is taken into account in the simulation. Since the fit does not improve if two equivalent Cl nuclei are considered, we are not in the position to establish directly the number of coordinated chloride ligands. Given the high complexity of the system and the contribution of multiple conformers the quality of the simulations seems acceptable for practical purposes even though the simulated spectra do not reproduce the experimental data perfectly.
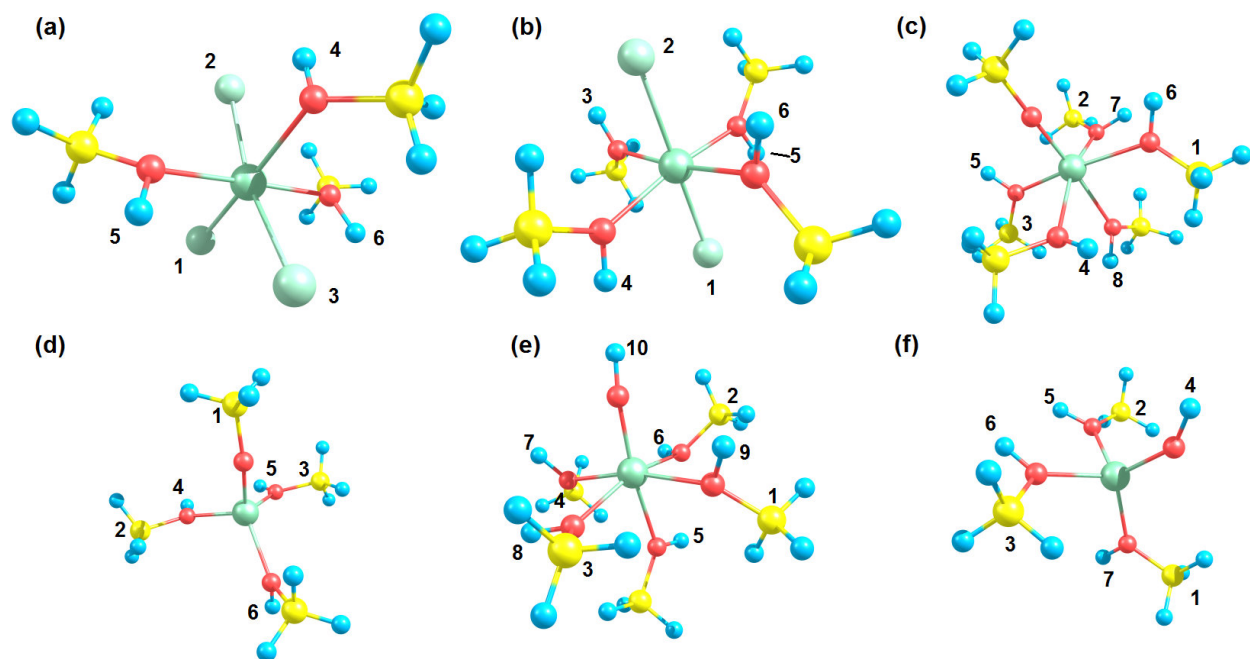
Fig. 4 Optimized structures used for calculating the hyperfine values (a) $Ti(CH_3OH)_3Cl_3$, (b) $[Ti(CH_3OH)_4Cl_2]^+$, (c) $[Ti(CH_3OH)_5(OCH_3)]^{2+}$, (d) $[Ti(CH_3OH)_3(OCH_3)]^{2+}$, (e) $[Ti(CH_3OH)_5(OH)]^{2+}$, (f) $[Ti(CH_3OH)_3(OH)]^{2+}$.

Computational modeling

To relate the experimental EPR parameters to local structural parameters of the different possible Ti(III) complexes the **g** and **A** tensors for a representative selection of Ti(III) complexes shown in Figure 4 was carried out. The models were chosen based on the present experimental findings and previous literature assignments.[6-9] In particular the tetrahedral structures of Figure 4d and f have been included based on the assignment of Ref.9.

Computed g values for the different complexes shown in Figure 4 are listed in Table 3. Examination of Table 3 shows that the computed g values for both chloride-containing complexes ($Ti(CH_3OH)_3Cl_3$ and $[Ti(CH_3OH)_4Cl_2]^+$) are characterized by a fairly large **g** anisotropy ($\Delta g=g_{max}-g_{min}$). Both sets of data are in good agreement with the experimentally determined **g** tensor of species 1, with the $[Ti(CH_3OH)_4Cl_2]^+$ complex giving a better fit. Species 1 has been demonstrated, by means of HYSCORE, to have directly coordinated chlorine nuclei, however the number of ligated Cl cannot be determined from the spectra. We remark that in the experiment we expect to have a combination of different conformers, indeed the DFT computations show that a variation in the number of chloride ligands may explain the broad EPR lines (strain) of Species 1 observed experimentally.

Table 3 DFT computed **g** tensors for the complexes illustrated in Figure 4 compared with the experimental values.

		g_x	g_y	g_z	Δg ($g_{max} - g_{min}$)
DFT	$Ti(CH_3OH)_3Cl_3$	1.9234	1.9450	1.9849	0.0615
	$[Ti(CH_3OH)_4Cl_2]^+$	1.8437	1.9532	1.9880	0.1443
	$[Ti(CH_3OH)_5(OCH_3)]^{2+}$	1.9607	1.9773	1.9815	0.0208
	$[Ti(CH_3OH)_3(OCH_3)]^{2+}$	1.9510	1.9802	1.9730	0.0292
	$[Ti(CH_3OH)_5(OH)]^{2+}$	1.9591	1.9759	1.9811	0.0220
	$[Ti(CH_3OH)_3(OH)]^{2+}$	1.9536	1.9816	1.9855	0.0319
Exp.	Species 1	1.830	1.889	1.978	0.148
	Species 2	1.942	1.962	1.962	0.020

Analysis of the DFT-computed hyperfine parameters (Table 4) indicates that a common feature of directly coordinated chlorines for all $[TiCl_n(CH_3OH)_{6-n}]^{(3-n)+}$ species is the dominant dipolar nature of the Cl hyperfine tensors, indicating a large fraction of spin density transfer into the Cl 3p orbitals. The HYSCORE experiments confirm this large hyperfine anisotropy (Table 2). Directly coordinated Cl ligands are also characterized by quadrupole couplings (e^2qQ/h) in the range 13-15 MHz with the principal axes of the hfi and nqi tensors nearly coincident. The best fit of the experimental spectra provided a slightly lower e^2qQ/h value of the order of 10 MHz. Finally for both models the ^{1}H computed hyperfine couplings for the OH methanol protons, which give the large hyperfine couplings, show good agreement with the experimental value, in particular for the $[Ti(CH_3OH)_4Cl_2]^+$ complex. Considering that thermally averaged parameters are likely to be measured in the experiment, the two models shown in Figure 4a and 4b can be considered as representative of the complexes with general formula $[TiCl_n(CH_3OH)_{6-n}]^{(3-n)+}$ with n ranging from 0 to 2, that are responsible for the EPR spectrum of Species 1 and the spectrum observed for $TiCl_3$/MeOH.

Table 4 DFT-computed ^{35}Cl and ^1H hyperfine and ^{35}Cl quadrupole tensors for the complexes illustrated in Figure 4a and 4b. Only the OH protons, which give the largest *hfi* couplings, are reported. The numbering of the atoms is given in Figure 4. All *hfi* and *nqi* values are in MHz, Euler angles are in degree.

Model		A_x	A_y	A_z	α,β,γ	e^2qQ/h	α',β',γ	η
	Cl1	-2.43	-0.42	-4.55	-2.7, +31, +7.3	+13.44	-7.7, +17.8, +15.5	0.10
	Cl2	+9.78	-7.43	-2.77	+31.5, +6.5, +67.4	+15.0	-26.3, +10.7, +33.7	0.06
	Cl3	-7.79	+8.44	-3.90	-8.5, +23, +14.4	+14.6	-29.3, +30.1, +37.4	0.14
a	H4	-3.86	-3.26	+8.13	-2.8, +41.6, +5.2	-	-	-
	H5	+5.43	+18.73	+5.21	+6.8, +61.4, +23.1	-	-	-
	H6	+4.57	+17.77	+4.36	-10.8, +57.7, -7.2	-	-	-
	Cl1	+11.46	-5.17	-9.45	-6.1, +87.7, -1.3	+13.5	-7.9, +87.6, -1.1	0.63
	Cl2	+12.34	-4.95	-9.58	-13.9, +87.9, +0.1	+13.8	-12.7, +87.7, -0.4	0.62
	H3	+0.15	-0.21	+12.06	-10.7, +45.1, -64.6	-	-	-
b	H4	+14.06	+1.67	+1.90	+12, +35.2, -78.1	-	-	-
	H5	+1.70	+1.46	+13.95	+3.5, +54.5, +65.9	-	-	-
	H6	+12.22	+0.39	+0.01	+44.4, +68.4, -10.8	-	-	-

a = $Ti(CH_3OH)_3Cl_3$; b=$[Ti(CH_3OH)_4Cl_2]^+$

The second species (species 2) is characterized by a small anisotropy and was clearly demonstrated to have no directly coordinated Cl^- ions. Different authors[6,9,10,29] suggested that the low anisotropic spectrum is characterized by the presence of directly coordinated hydroxy or methoxy groups. To verify these hypotheses we computed the EPR properties of different Ti(III) complexes characterized by different symmetries with OH^- or CH_3O^- as directly coordinated ions.

Examination of Table 3 shows that indeed a common feature to all these models (Figure 4 c-f) is the reduced anisotropy of the *g* tensor with respect to the previous case (see reduced Δg). From the experimental values reported in Table 1, we see that for the experimental species 1 $\Delta g = 0.148$, while for species 2 $\Delta g = 0.02$. Comparison with the computed Δg values in Table 3 shows that indeed the coordination of charged hydroxy or methoxy groups is a likely origin of the reduced *g* anisotropy observed experimentally for species 2. In the case of 6-fold coordinated complexes (Figure 4c and 4e) the substitution of a CH_3O^- with an OH^- group leads to only small variations in the computed *g* tensors. The tetrahedral complexes show a similar trend, although the overall anisotropy (Δg) is slightly higher (Table 3). In contrast to the *g* tensor trend, the ^1H *hfi* values for the 6-fold coordinated (Figure 4c and 4e) and 4-fold coordinated models (Figures 4d and 4f) show consistent differences (Table 5). In particular for the Ti(III) complexes with tetrahedral symmetry large proton *hfi* values, with a large Fermi contact contribution, are computed, clearly at variance with the experimental results. The same trend is observed for the ^{13}C coupling for which a maximum value of approximately 6 MHz and an a_{iso} of the order of 4.5 MHz has been obtained experimentally (Table 2). The computed ^{13}C coupling constants for both the 6-fold coordinated complexes are in line with these values, while exceedingly large values are obtained for the 4-fold coordinated models (Table 5). The assignment of a spectrum analogous to that of species 2 to an hydroxy Ti(III) complex in tetrahedral symmetry was proposed by ref. 9. Our calculations, however do not support this model, favoring the 6-fold coordinated complex, which is the expected coordination for Ti(III) in solution.

Based on these results the two species observed in the EPR spectrum can be associated to two distinct families of solvated Ti(III) ions. The broad anisotropic component (Species 1) is associated to complexes containing directly ligated Cl nuclei of general formula $[TiCl_n(CH_3OH)_{6-n}]^{(3-n)+}$ with *n* ranging from 0 to 2. The narrow component has to be assigned to either hydroxy or methoxy Ti(III) complexes generated by H_2O or CH_3OH hydrolysis, the presence of directly coordinated OH^- or CH_3O^- groups being responsible for the low anisotropy of the EPR spectrum. It is important to note that similar spectra are observed in activated model Ziegler-Natta catalysts. The observation of the narrow component in these samples suggests the presence of hydroxyl and/or alkoxy groups in close proximity to the Ti(III) ions in the model $MgCl_2/TiCl_4$ Ziegler-Natta catalyst. We remark that these narrow components represent a

minor fraction (approximately 5%) of the Ti(III) EPR active species, which in turn are only a small part of the overall Ti; we trace them to the presence of adventitious water contaminating the pre-catalyst.

Conclusions

Advanced EPR experiments combined with DFT modelling have been applied to the study of $TiCl_3$ dissolved in anhydrous and hydrated methanol. The EPR spectrum of the solvated Ti(III) species is the convolution of two different species characterized by distinctly different *g* tensors with different anisotropies. The highly anisotropic species (species 1) is found to be largely dominating in the absence of water (absolute methanol) and is characterized by distinct [35,37]Cl *hfi* in the HYSCORE spectrum, which are resolved for the first time. DFT modeling allows to assign the experimentally observed Cl *hfi* to chloride ions directly coordinated to Ti(III) ions. The presence of water promotes an increment of the second species (species 2) characterized by a much lower *g* anisotropy and the absence of directly coordinated chlorine ions. Comparison of the experimentally determined spin Hamiltonian parameters with DFT-computed values allows establishing that the origin of the reduced anisotropy is the direct coordination of either OH^- or CH_3O^- groups formed by hydrolysis of coordinated water molecules as postulated by Kuchmii *et al*.[9] However, differently from the claims made by ref. 9, we found that the coordination of the Ti(III) ions is octahedral and not tetrahedral. When $TiCl_3$ is dissolved in methanol in the presence of water the following equilibria can thus be written $[TiCl_n(CH_3OH)_{6-n}]^{(3-n)+}$ (with *n* ranging from 0 to 2) $\leftrightarrows$ $[Ti(CH_3OH)_5(OH)]^{2+}$ $\leftrightarrows$ $[Ti(CH_3OH)_5(OCH_3)]^{2+}$, where the first general complex accounts for the anisotropic EPR spectrum (species 1), while the hydroxy/metoxy complexes are responsible for the narrow EPR signal (species 2).

Similar EPR spectra have been observed in the case of a $MgCl_2$-supported Ti-based Ziegler-Natta model catalyst activated with TEA vapors. In particular also in the case of the solid state catalyst, two EPR-active species are observed, characterized by *g* tensors very similar to species 1 and 2 observed in frozen solutions. This analogy supports the concept of the solid support ($MgCl_2$) as a solid polar solvent where Ti ions are incorporated as the solute. The observation of the low anisotropic EPR signal (species 2), analogous to that of the hydroxy or methoxy complexes, in the activated model catalysts, suggests that OR^- (or possibly even OH^-, whose presence is less likely in the activated catalyst) groups, are directly coordinated to Ti(III) ions. The EPR signal of species 2 can thus be taken as diagnostic for the presence of coordinated oxo groups, at concentrations that may escape other analytical techniques. The presence of such groups is likely originated from water contamination of the pre-catalyst and subsequent reaction with the alkyl-aluminium activator.

Overall, this study demonstrates that a combination of advanced EPR methods in conjunction with DFT calculations has a great potential in gaining structural information on Ti(III) systems, in particular in the context of the study of complex heterogeneous Ziegler-Natta catalysts, as will be shown in forthcoming papers.

Acknowledgements

Notes and references

[a] *University of Antwerp, Department of Physics, Universiteitsplein 1, B-2610 Wilrijk, Belgium; E-mail: sabine.vandoorslaer@uantwerpen.be*

[b] *Dipartimento di Chimica, University of Torino Via Giuria, 7 - 10125 Torino, Italy. ; E-mail: mario.chiesa@unito.it*

[c] *Dutch Polymer Institute (DPI), P.O. Box 902, 5600 AX Eindhoven, The Netherlands.*

[d] *Dipartimento di Scienze Chimiche, Università degli Studi di Napoli Federico II, Via Cintia, 80126 Napoli, Italy.*

† Electronic Supplementary Information (ESI) available: CW-EPR spectra of $TiCl_3$ in anhydrous methanol, DFT-computed [47]Ti *hfi* tensor, field dependent 2-pulse ESEEM experiments, EPR spectra of $TiCl_3$ solutions at different concentrations, HYSCORE simulations. See DOI: 10.1039/b000000x/

1   G. Natta, P. Corradini and G. Allegra, *J. Polym. Sci.* 1961, **51**,399.

2   J. Boor Jr, *Ziegler-Natta catalysts and polymerization, Academic Press, 1979.*

3   D. Gourier and E. Samuel, *J. Am. Chem. Soc.*, 1987, **109**, 4571; M. Horáček, V. Kupfer, U. Thewalt, M. Polašek and K. Mach, *J. Organomet. Chem.* 1999, **579**, 126; A. M. Prakash, L. Kevan, M. H. Zahedi-Niaki and S. Kaliaguine, *J. Phys. Chem. B*, 1999, **103**, 831; M. Aono and R. R. Hasiguti, *Phys. Rev. B*, 1993, **48**, 12406; R. F. Howe and M. Grätzel, *J. Phys. Chem.*, 1985, **89**, 4495; S. Van Doorslaer, J. J. Shane, S. Stoll, A. Schweiger, M. Kranenburg and R. J. Meier, *J. Organomet. Chem.*, 2001, **634**, 185.

4   S. Maurelli, S. Livraghi, M. Chiesa, E. Giamello, S. Van Doorslaer, C. Di Valentin and G. Pacchioni, *Inorg. Chem.*, 2011, **50**, 2385.

5   A. Cangönül, M. Behlendorf, A. Gansäuer and M. van Gastel, *Inorg. Chem.*, 2013, **52**, 11859.

6   W. Giggenbach and G. H. Brubaker, *Inorg. Chem.*, 1969, **8**, 1131.

7   J. B. Raynor and A. W. L. Ball, *Inorg. Chim. Acta*, 1973, **7**, 315.

8   S. G. Carr and T. D. Smith, *J. Chem. Soc., Dalton Trans.*, 1972, 1887.

9   S. Ya. Kuchmii, A. V. Korzhak and A. I. Kryukov, *Theoretical and Exp. Chem.*, 1984, **19**, 544.

10   E. L. Waters, A. H. Maki, *Phys. Rev.*, 1962, **125**, 233.

11   E. L. Klein, A. V. Astashkin, D. Ganyushin, C. Riplinger, K. Johnson-Winters, F. Neese, and J. H. Enemark, *Inorg. Chem.* 2009, **48**, 4743.

12   P. J. Desrochers, K. W. Nebesny, M. J. LaBarre, S. E. Lincoln, T. M. Loehr, J. H. Enemark, *J. Am. Chem. Soc.,* 1991, **113**, 9193.

13   A. Auriemma, V. Busico, P. Corradini, M. Trifuoggi, *Eur. Polym. J.*, 1992, **28**, 513; V. Busico, P. Corradini, L. De Martino, A. Proto, V. Savino, E. Albizzati, *Makromol. Chem.* 1985, **186**, 1279.

14   P. Höfer, A. Grupp, H. Nebenführ and M. Mehring, *Chem. Phys. Lett.*, 1986, **132**, 279.

15   S. Stoll and A. Schweiger *J. Magn. Reson.* 2006, **178**, 42.

16   F. Neese, *J. Chem. Phys.*, 2001, **115**, 11080; F. Neese, *J. Phys. Chem. A*, 2001, **105**, 4290; F. Neese, *J. Chem. Phys.*, 2003, **118**, 3939; F. Neese, *J. Chem. Phys.,* 2005, **122**, 034107/1.

17   J. P. Perdew, *Phys. Rev. B*, 1986, **33**, 8822-8824; J. P. Perdew, *Phys. Rev. B*, 1986, **34**, 7406-7406; A. D. Becke, *Phys. Rev. A*, 1988, **38**, 3098.

18   A. Schäfer, H. Horn and R. Ahlrichs, *J. Chem. Phys.*, 1992, **97**, 2571; The Ahlrichs (2df,2pd) polarization functions were obtained from the TurboMole basis set library under ftp.chemie.uni-karlsruhe.de/pub/basen, R. Ahlrichs and co-workers (unpublished).

19   T. C. DeVore and W. Weltner, Jr., *J. Am. Chem. Soc.*, 1977, **99**, 4700.

20   C. Adamo and V. Barone, *J. Chem. Phys.*, 1999, **110**, 6158.

21   The Ahlrichs (2df,2pd) polarization functions were obtained from the TurboMole basis set library under ftp.chemie.uni-karlsruhe.de/pub/basen, R. Ahlrichs and co-workers (unpublished).

22   V. Barone in *Recent Advances in Density Functional Methods*, ed. D. P. Chong, World Scientific Publ. Co., Singapore, 1996, pp. 287.

23   S. Sinnecker, A. Rajendran, A. Klamt, M. Diedenhofen and F. Neese, *J. Phys. Chem. A*, 2006, **110**, 2235.

24   J. Lewis, D. J. Machin, I. E. Newnham and R. S. Nyholm, *J. Chem. Soc.* 1962, 2036; J. A. Watts *Inorg. Chem.* 1966, **5**, 281.

25   J. C. W. Chien and J.-C. Wu *J. Polymer Sci.* 1982, **20**, 2461.

26   P. Brant and A. N. Speca, *Macromolecules* 1987, **20**, 2740.

27   P, Ballinger, F. A. Long, *J. Am. Chem. Soc.* 1960**, 82**, 795; H. I. Abrash, *J. Chem. Educ.* 2001, **78**, 1496.

28   P. Chaudhuri and H. Diebler, *J. Chem. Soc., Dalton Trans.*, 1977, 596; R. L. Pecsok and A. N. Fletcher, *Inorg. Chem.*, 1962, **1**, 155; M. Hartmann, T. Clark and R. van Eldik, *J. Phys. Chem. A*, 1999, **103**, 9899.

29   I. B. Goldberg and W. F. Goeppinger, *Inorg. Chem.*, 1972, **11**, 3129.